

Comparison of gas sensing properties based on hollow and porous α -Fe₂O₃ nanotubes

Xuexin Guo¹ · Jinbao Zhang¹ · Mucui Ni¹ · Li Liu¹ · Hongwei Lian¹ · Han Wang¹

Received: 29 April 2016 / Accepted: 23 June 2016 / Published online: 30 June 2016
© Springer Science+Business Media New York 2016

Abstract Hollow and porous α -Fe₂O₃ nanotubes were successfully synthesized by single nozzle electrospinning method followed by annealing treatment. The crystal structures and morphologies of the as-prepared materials were characterized by X-ray diffraction and scanning electron microscopy, respectively. The as-prepared materials were applied to construct gas sensor devices which gas sensing properties were further investigated. The obtained results revealed that porous α -Fe₂O₃ nanotube gas sensors exhibit a markedly enhanced gas sensing performance compared with hollow α -Fe₂O₃ nanotube gas sensors, which was about three times higher to 100 ppm acetone at 240 °C. Interestingly, hollow and porous α -Fe₂O₃ nanotube gas sensors both showed fast response–recovery time and good selectivity, but the porous ones possessed the shorter recovery time. The improved properties could be attributed to the unique morphology of porous nanotubes. Thus, further improvement of performance in metal-oxide-semiconductors materials could be realized by preparation the unique porous structures of nanotubes. Moreover, it is expected that porous metal-oxide-semiconductors nanotubes could be further design as promising candidates for gas sensing materials.

1 Introduction

Over the past decades, metal-oxide-semiconductors (MOS) such as SnO₂ [1], ZnO [2], TiO₂ [3], In₂O₃ [4] and Fe₂O₃ [5] have attracted considerable attention as gas sensing materials due to their convenience and simplicity in synthesis. Among them, α -Fe₂O₃ has been widely studied as gas sensing material owing to its low-cost, high thermal/chemical stability and non-toxic [6]. As a typical n-type transition MOS, α -Fe₂O₃ has a narrow band gap of 2.2 eV, which might contribute to form a higher conduction band position [7]. Nevertheless, they usually suffer from several drawbacks such as poor sensitivity, slow response–recovery time and so on.

Up to date, significant efforts have been made to overcome these limitations [8, 9]. As we know, the structure and surface morphology of MOS materials strongly affect their properties [10]. Therefore, various structures of iron oxide have been synthesized by many methods to improve their performance [11–13]. For instance, Atar et al. successfully fabricated a novel magnetic Fe@Au core–shell nanoparticle which was applied in catalytic reductions of 4-nitrophenol and 2-nitrophenol in the presence of sodium borohydride [14]. Nanoflower structured α -Fe₂O₃ has been reported which exhibits high electrochemical sensing and photocatalytic property [15]. These special structures and morphologies make the iron oxide has excellent performance in many fields. Currently, one-dimensional nanostructures materials such as nanofibers [16], nanobelts [17], nanorods [18] and nanotubes [19] have attracted extensive attention. Owing to the large length-to-diameter ratio which is conducive to electronic transmission, one-dimensional nanomaterials show good prospect in the field of gas sensor. For example, Zheng et al. [16] constructed In₂O₃ nanofibers which exhibited highly sensitive to

✉ Li Liu
liul99@jlu.edu.cn

¹ State Key Laboratory of Superhard Materials, College of Physics, Jilin University, Changchun 130012, People's Republic of China

ethanol. Kruefu et al. [20] prepared the Ru-functionalized WO_3 nanorods as ultra-sensitive H_2S gas sensors via a hydrothermal method. With a high surface-to-volume ratio, the hollow nanostructure generally has better performance compared with other one-dimensional nanostructures [21–23]. However, in general, we could get nanofibers, nanobelts and nanotubes through electrospinning method. Forming a large number of pores on nanotubes is difficult. Successfully preparing porous nanotubes and using in the direction of gas sensors is rarely reported. Moreover, to the best of our knowledge, there has been no study on the comparison of hollow nanotubes and porous nanotubes for gas sensing materials.

In this work, hollow $\alpha\text{-Fe}_2\text{O}_3$ nanotubes and porous $\alpha\text{-Fe}_2\text{O}_3$ nanotubes have been synthesized by electrospinning method with following annealing process. Moreover, the gas sensing properties of the sensors based on these nanostructures have been mainly investigated, and the obtained results demonstrated that the porous structure of nanotubes has a positive effect on gas sensitivity.

2 Experimental

All chemical reagents were analytical grade and used without further purification. Polyvinyl pyrrolidone (PVP, Mw = 1,300,000) was obtained from Sigma-Aldrich (USA). $\text{Fe}(\text{NO}_3)_3 \cdot 9\text{H}_2\text{O}$ (99.99 %), *N,N*-dimethylformamide (DMF ≥ 99.5 %) and ethanol (≥ 99.7 %) were purchased from Aladdin (Shanghai, China).

2.1 Synthesis of materials

In a typical synthesis, 0.4 g $\text{Fe}(\text{NO}_3)_3 \cdot 9\text{H}_2\text{O}$ was dissolved in 3 g DMF with vigorous stirring. Subsequently, 0.5 g PVP and 4.5 g ethanol were added into the mixture solution with stirring for 8 h. Then a homogeneous solution was obtained. Next, the precursor solution was loaded into a plastic syringe that was equipped with a stainless steel nozzle and electrospun at a DC voltage of 18 kV with a flow rate of 1.0 mL h^{-1} . The non-woven collector mats were placed at a distance of about 20 cm from the capillary. Finally, the as-collected films were annealed in a tube furnace at $550 \text{ }^\circ\text{C}$ for 3 h with a rate of 2 and $10 \text{ }^\circ\text{C min}^{-1}$ to form hollow and porous nanotubes, respectively.

2.2 Characterization of products

X-ray diffraction (XRD) patterns were obtained on an XRD-6000 X-ray diffractometer (XRD, Shimadzu, Kyoto, Japan) with $\text{Cu K}\alpha$ 1 radiation ($\lambda = 1.5406 \text{ \AA}$). Scanning electron microscope (SEM) images were obtained using an FEI XL30 instrument. The gas sensing properties of the

sensors were measured by a CGS-8 intelligent gas-sensing analysis system (Beijing Elite Tech Co., Ltd., Beijing, China).

2.3 Gas sensor fabrication and measurement

The gas sensors were achieved as follows: the obtained sample was slightly grinded and mixed with a small amount of deionized water (about at a weight ratio of 4:1) to form a paste. Then, the resulting paste was coated on the surface of a ceramic tube which was previously printed a pair of Au electrodes and Pt conducting wires [24]. And a Ni–Cr alloy heating wire was inserted in the ceramic tube as a heater which controls the variation of the working temperature. The gas sensor response (*S*) to the target gas is defined as the ratio $S = R_a/R_g$, where R_a and R_g are the resistance of the sensor in air and in target gas, respectively. The response time and recovery time are defined as the time taken by the sensor to achieve 90 % of the total resistance changes upon exposure to target gas and air, respectively.

3 Results and discussion

3.1 Structural and morphological characteristics

The crystallinities of the as-prepared nanotubes were investigated by XRD analysis. Figure 1 shows that all of the prominent diffraction peaks of both samples are indexed to a pure rhombohedral phase of $\alpha\text{-Fe}_2\text{O}_3$ (JCPDS Card No. 33-0664). The diffraction peaks at 24.15° , 33.3° , 35.8° , 40.6° , 49.4° , 54.1° , 57.4° , 62.3° , 63.9° and 71.9° correspond to the (012), (104), (110), (113), (024), (116), (122), (214), (030) and (220) planes. The intensity of the characteristic peak is strong, indicating a highly crystalline

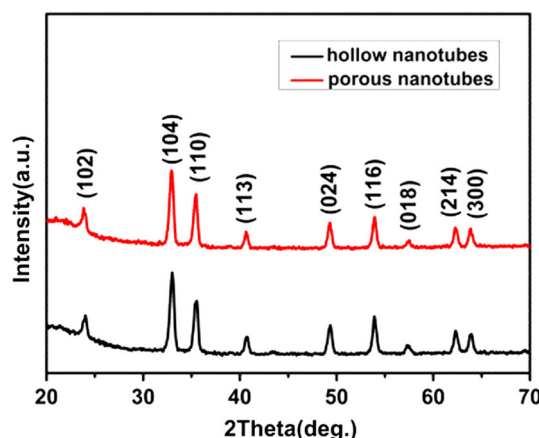


Fig. 1 XRD patterns of hollow $\alpha\text{-Fe}_2\text{O}_3$ nanotubes and porous $\alpha\text{-Fe}_2\text{O}_3$ nanotubes

structure. No characteristic peaks are observed for other impurities, indicating the high purity of both samples.

The morphology of the obtained α -Fe₂O₃ nanomaterials were characterized by SEM analysis. As shown in Fig. 2a, b, the hollow α -Fe₂O₃ nanotubes are relatively uniform with the diameter of 100 nm and without any pores on the surface. Figure 2c, d display the porous α -Fe₂O₃ nanotubes. It can be observed that there are many irregular pores on the surface. The diameter has a small level of growth, reaching about 120 nm.

3.2 Gas sensing properties

It is well known that the operating temperature plays an important role in gas sensors. In order to find the optimum operating temperature, the responses of hollow and porous α -Fe₂O₃ nanotube gas sensors to 100 ppm acetone were investigated. The results are shown in Fig. 3. It can be observed that the responses of the two kinds of gas sensors show the same tendency, increasing to their highest values at 240 °C and decreasing with a further rise of the operating temperature. This performance can be explained as follows. With the operating temperature reaching the optimum value, the oxygen adsorption and desorption reaction on the surface of the samples achieves a balance, gradually. Therefore, the response reaches its maximum value. With the operating temperature further increases, the response value decreases because the desorption is stronger than adsorption [25]. Hence, 240 °C is chosen as the optimum operating temperature. The sensor based on porous α -Fe₂O₃ nanotubes exhibits higher response of 11 at 240 °C, which is about three times than that of hollow α -Fe₂O₃ nanotubes. The experimental result shows that porous α -Fe₂O₃ nanostructure can obviously improve the sensitivity to acetone.

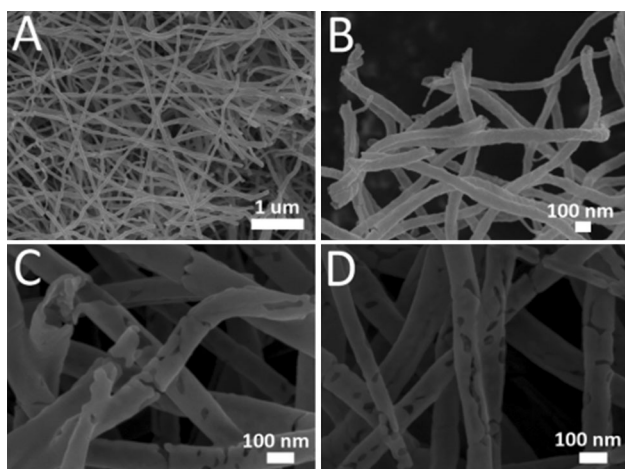


Fig. 2 SEM images of hollow α -Fe₂O₃ nanotubes (a, b) and porous α -Fe₂O₃ nanotubes (c, d)

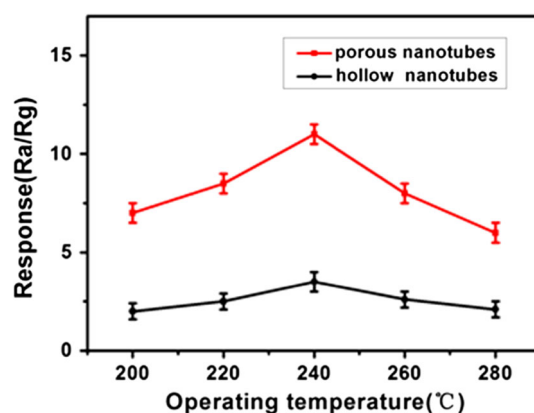


Fig. 3 The response curves of hollow α -Fe₂O₃ nanotube and porous α -Fe₂O₃ nanotube gas sensors to 100 ppm acetone at different operating temperatures

The response and recovery curves of hollow α -Fe₂O₃ nanotube and porous α -Fe₂O₃ nanotube gas sensors to 100 ppm acetone at 240 °C are presented in Fig. 4. The curves show the similar tendencies. The response times are both 9 s. The recovery times of hollow and porous nanotube gas sensors are 8 and 3 s, respectively. The results indicate that both sensors own fast response–recovery time, but porous nanotube gas sensor possesses shorter recovery time. This phenomenon could be attributed to abundant pores on the surface of materials, which could improve the adsorption and desorption rate of gas molecules.

The hollow and porous α -Fe₂O₃ nanotube gas sensors were exposed to different concentrations of acetone at 240 °C in order to further test their sensitivities. The results presented in Fig. 5. It can be observed that sensor based on porous α -Fe₂O₃ nanotubes in each concentration exhibited higher response than that of hollow α -Fe₂O₃ nanotubes. The responses of hollow α -Fe₂O₃ nanotube gas sensor to

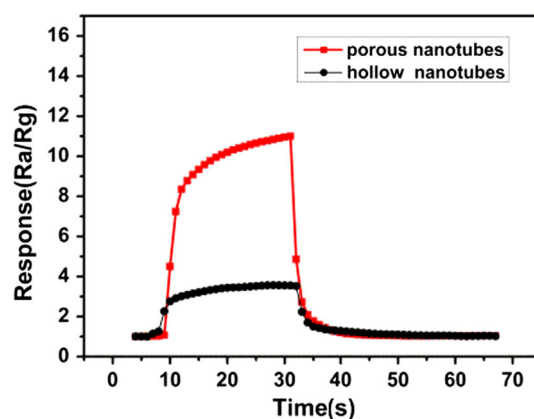


Fig. 4 The response and recovery curves of hollow α -Fe₂O₃ nanotube and porous α -Fe₂O₃ nanotube gas sensors to 100 ppm acetone at 240 °C

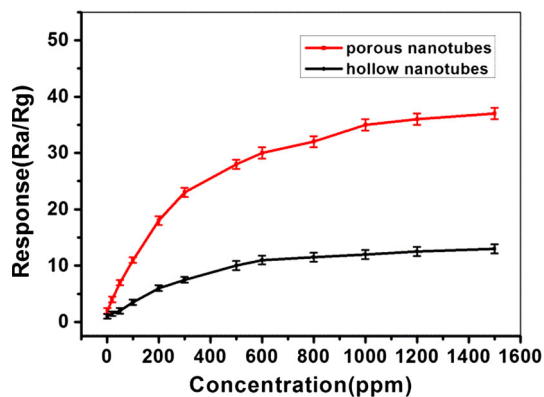


Fig. 5 The response curves of hollow $\alpha\text{-Fe}_2\text{O}_3$ nanotube and porous $\alpha\text{-Fe}_2\text{O}_3$ nanotube gas sensors to different concentration of acetone at 240 °C

50, 100, 300 and 500 ppm acetone are about 2, 3.5, 7.5 and 10, respectively. The responses of porous $\alpha\text{-Fe}_2\text{O}_3$ nanotube gas sensor to 50, 100, 300 and 500 ppm acetone are about 7, 11, 23 and 28, respectively. The response of porous $\alpha\text{-Fe}_2\text{O}_3$ nanotube gas sensor is almost linear from 1 and 200 ppm, revealing a good linear characteristic of sensor. Then the response increases slowly and gradually saturated with the acetone concentration increased. That phenomenon could be explained by the fact that no chemisorbed oxygen species on the surface of porous nanotubes can further react with acetone molecules.

The selectivity is another important parameter in evaluating the performance of a gas sensor. The poor selectivity would cause a false alarm, which would imprison its applications. Therefore, the two kinds of gas sensors were exposed to acetone ($\text{C}_3\text{H}_6\text{O}$), ethanol ($\text{C}_2\text{H}_5\text{OH}$), formaldehyde (HCHO), ammonia ($\text{NH}_3\cdot\text{H}_2\text{O}$), carbon monoxide (CO), methane (CH_4), hydrogen (H_2) and

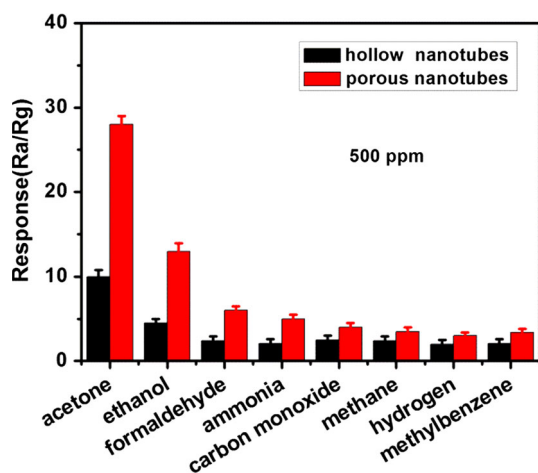
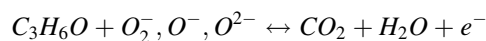
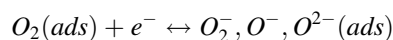
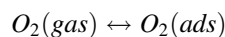


Fig. 6 The responses of hollow and porous $\alpha\text{-Fe}_2\text{O}_3$ nanotube gas sensors to different gases at 240 °C

methylbenzene(C_7H_8) under the same condition. Figure 6 shows that the sensors both exhibit the highest response to acetone, moderate response to ethanol, low responses to formaldehyde, ammonia, carbon monoxide, methane, hydrogen and methylbenzene. As is known, acetone and ethanol are difficult to distinguish due to their similar chemical nature [26]. In this work, the responses of hollow $\alpha\text{-Fe}_2\text{O}_3$ nanotube gas sensor to 500 ppm acetone and ethanol are 10 and 4.6, respectively. The responses of porous $\alpha\text{-Fe}_2\text{O}_3$ nanotube gas sensor to 500 ppm acetone and ethanol are 28 and 13, respectively. Therefore, ethanol and acetone can be easily distinguished. The results indicate that the two kinds of gas sensors both possess good selective ability to acetone. Meanwhile, porous $\alpha\text{-Fe}_2\text{O}_3$ nanotube gas sensor has higher sensitivity to acetone at the same concentration. Therefore, porous $\alpha\text{-Fe}_2\text{O}_3$ nanotubes could be a promising candidate for detecting acetone. The response values to different gases have such great difference may be attributed to the characteristics of the gas sensing materials and the operating temperature. Previous studies have demonstrated that different gases need different energies for adsorption, desorption and reaction on the surface of the gas sensing materials [27].

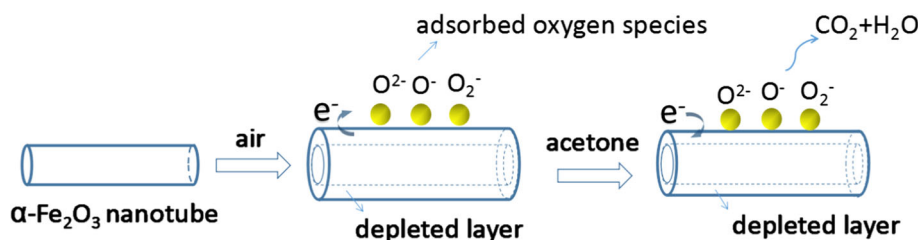
3.3 Gas sensing mechanism

Generally, the most widely accepted theory of gas sensing mechanism is the adsorption and desorption process of oxygen molecules on the surface of materials [28, 29]. As a typical n-type transition MOS, the gas sensing mechanism of $\alpha\text{-Fe}_2\text{O}_3$ can be divided into adsorption, charge transfer and desorption. When the sensor exposed to air, the atmospheric oxygen molecules (O_2) are adsorbed on the surface and capture free electrons from conducting band to form chemisorbed oxygen species. Owing to the electrons are captured, the electron density decreases, leading to a higher surface resistance. When the sensor exposed to the target gas, the target gas molecules are adsorbed onto the surface and react with the previously chemisorbed oxygen species. The trapped electrons will be released back to the sensing materials, which results in a decrease of resistance. The reaction process could be described by following equations and Fig. 7.



The enhanced gas sensing performance of porous $\alpha\text{-Fe}_2\text{O}_3$ nanotube gas sensors could be attributed to following two factors. On the one hand, the unique porous structure could increase the surface area of materials and provide more active sites for adsorption and desorption of

Fig. 7 A simple sketch map of the adsorption, desorption, and reactions of oxygen species and acetone on the sample surface



gas molecules. On the other hand, the porous structure can improve the transmission rate of gas molecules.

4 Conclusion

In summary, hollow $\alpha\text{-Fe}_2\text{O}_3$ nanotubes and porous $\alpha\text{-Fe}_2\text{O}_3$ nanotubes were successfully prepared by electrospinning method followed by annealing treatment. The as-prepared nanostructures were investigated as gas sensing materials. The obtained results indicated that porous $\alpha\text{-Fe}_2\text{O}_3$ nanotube gas sensors exhibit higher sensitivity and short recovery time. The response of gas sensors based on porous $\alpha\text{-Fe}_2\text{O}_3$ nanotubes is 11–100 ppm acetone, which is three times larger than that of hollow $\alpha\text{-Fe}_2\text{O}_3$ nanotubes (3.5). The response times of the two kinds of gas sensors are both 9 s and the recovery times are 8 and 3 s, respectively. The enhanced properties are related to the unique porous structures. The preliminary study in this work reveals that forming pores on metal oxide semiconductors can further enhance the performance of gas sensors.

Acknowledgments The work has been supported by the Jilin Provincial Science and Technology Department (No. 20140204027GX).

References

1. K.-M. Li, Y.-J. Li, M.-Y. Lu, C.-I. Kuo, L.-J. Chen, Direct conversion of single-layer SnO nanoplates to multi-layer SnO₂ nanoplates with enhanced ethanol sensing properties. *Adv. Funct. Mater.* **19**, 2453–2456 (2009)
2. S. Benkara, S. Zerkout, H. Ghamri, Synthesis of Sn doped ZnO/TiO₂ nanocomposite film and their application to H₂ gas sensing properties. *Mater. Sci. Semicond. Process.* **16**, 1271–1279 (2013)
3. L. Wang, J. Deng, Z. Lou, T. Zhang, Cross-linked p-type Co₃O₄ octahedral nanoparticles in 1D n-type TiO₂ nanofibers for high-performance sensing devices. *J. Mater. Chem. A* **2**, 10022 (2014)
4. P. Song, Q. Wang, Z. Yang, Biomorphic synthesis and gas response of In₂O₃ microtubules using cotton fibers as templates. *Sens. Actuators B Chem.* **168**, 421–428 (2012)
5. N.D. Cuong, D.Q. Khieu, T.T. Hoa, D.T. Quang, P.H. Viet, T.D. Lam, N.D. Hoa, N.V. Hieu, Facile synthesis of $\alpha\text{-Fe}_2\text{O}_3$ nanoparticles for high-performance CO gas sensor. *Mater. Res. Bull.* **68**, 302–307 (2015)
6. P. Sun, C. Wang, X. Zhou, P. Cheng, K. Shimanoe, G. Lu, N. Yamazoe, Cu-doped $\alpha\text{-Fe}_2\text{O}_3$ hierarchical microcubes: synthesis and gas sensing properties. *Sens. Actuators B Chem.* **193**, 616–622 (2014)
7. Y. Guo, G. Zhang, J. Liu, Y. Zhang, Hierarchically structured $\alpha\text{-Fe}_2\text{O}_3/\text{Bi}_2\text{WO}_6$ composite for photocatalytic degradation of organic contaminants under visible light irradiation. *RSC Adv.* **3**, 2963 (2013)
8. N. Atar, Magnetic iron oxide and iron oxide@gold nanoparticle anchored nitrogen and sulfur-functionalized reduced graphene oxide electrocatalyst for methanol oxidation. *RSC Adv.* **5**, 26402–26409 (2015)
9. O. Akyıldırım, H. Medetalibeyoğlu, S. Manap, M. Beytur, F.S. Tokalı, M.L. Yola, N. Atar, Electrochemical sensor based on graphene oxide/iron nanoparticles for the analysis of quercetin. *Int. J. Electrochem. Sci.* **10**, 7743–7753 (2015)
10. W.X. Jin, S.Y. Ma, Z.Z. Tie, X.H. Jiang, W.Q. Li, J. Luo, X.L. Xu, T.T. Wang, Hydrothermal synthesis of monodisperse porous cube, cake and spheroid-like $\alpha\text{-Fe}_2\text{O}_3$ particles and their high gas-sensing properties. *Sens. Actuators B Chem.* **220**, 243–254 (2015)
11. M.L. Yola, T. Eren, N. Atar, Molecularly imprinted electrochemical biosensor based on Fe@Au nanoparticles involved in 2-aminoethanethiol functionalized multi-walled carbon nanotubes for sensitive determination of cefexime in human plasma. *Biosens. Bioelectron.* **60**, 277–285 (2014)
12. V.K. Gupta, M.L. Yola, T. Eren, F. Kartal, M.O. Çağlayan, N. Atar, Catalytic activity of Fe@Ag nanoparticle involved calcium alginate beads for the reduction of nitrophenols. *J. Mol. Liq.* **190**, 133–138 (2014)
13. N. Atar, T. Eren, M.L. Yola, H. Gerengi, S. Wang, Fe@Ag nanoparticles decorated reduced graphene oxide as ultrahigh capacity anode material for lithium-ion battery. *Ionics* **21**, 3185–3192 (2015)
14. V.K. Gupta, N. Atar, M.L. Yola, Z. Üstündağ, L. Uzun, A novel magnetic Fe@Au core-shell nanoparticles anchored graphene oxide recyclable nanocatalyst for the reduction of nitrophenol compounds. *Water Res.* **48**, 210–217 (2014)
15. R. Suresh, K. Giribabu, R. Manigandan, A. Vijayaraj, R. Prabu, A. Stephen, V. Narayanan, $\alpha\text{-Fe}_2\text{O}_3$ nanoflowers: synthesis, characterization, electrochemical sensing and photocatalytic property. *J. Iran. Chem. Soc.* **11**, 645–652 (2013)
16. W. Zheng, X. Lu, W. Wang, Z. Li, H. Zhang, Y. Wang, Z. Wang, C. Wang, A highly sensitive and fast-responding sensor based on electrospun In₂O₃ nanofibers. *Sens. Actuators B Chem.* **142**, 61–65 (2009)
17. U. Cvelbar, Z. Chen, M.K. Sunkara, M. Mozetič, Spontaneous growth of superstructure $\alpha\text{-Fe}_2\text{O}_3$ nanowire and nanobelt arrays in reactive oxygen plasma. *Small* **4**, 1610–1614 (2008)
18. H.-y. Yang, X.-L. Cheng, X.-F. Zhang, Z.-k. Zheng, X.-F. Tang, Y.-M. Xu, S. Gao, H. Zhao, L.-H. Huo, A novel sensor for fast detection of triethylamine based on rutile TiO₂ nanorod arrays. *Sens. Actuators B Chem.* **205**, 322–328 (2014)
19. C. Zhao, G. Zhang, W. Han, J. Fu, Y. He, Z. Zhang, E. Xie, Electrospun In₂O₃/ $\alpha\text{-Fe}_2\text{O}_3$ heterostructure nanotubes for highly sensitive gas sensor applications. *CrystEngComm* **15**, 6491 (2013)

20. V. Kruefu, A. Wisitsoraat, A. Tuantranont, S. Phanichphant, Ultra-sensitive H₂S sensors based on hydrothermal/impregnation-made Ru-functionalized WO₃ nanorods. *Sens. Actuators B Chem.* **215**, 630–636 (2015)
21. M.-Y. Liao, C.-C. Huang, M.-C. Chang, S.-F. Lin, T.-Y. Liu, C.-H. Su, C.-S. Yeh, H.-P. Lin, Synthesis of magnetic hollow nanotubes based on the Kirkendall effect for MR contrast agent and colorimetric hydrogen peroxide sensor. *J. Mater. Chem.* **21**, 7974 (2011)
22. C. Liu, X. Chi, X. Liu, S. Wang, Comparison of ethanol sensitivity based on cobalt–indium combined oxide nanotubes and nanofibers. *J. Alloys Compd.* **616**, 208–212 (2014)
23. W.-S. Kim, B.-S. Lee, D.-H. Kim, H.-C. Kim, W.-R. Yu, S.-H. Hong, SnO₂ nanotubes fabricated using electrospinning and atomic layer deposition and their gas sensing performance. *Nanotechnology* **21**, 245605 (2010)
24. L. Liu, C. Liu, S. Li, L. Wang, H. Shan, X. Zhang, H. Guan, Z. Liu, Honeycombed SnO₂ with ultra sensitive properties to H₂. *Sens. Actuators B Chem.* **177**, 893–897 (2013)
25. M. Hjiri, L. El Mir, S.G. Leonardi, A. Pistone, L. Mavilia, G. Neri, Al-doped ZnO for highly sensitive CO gas sensors. *Sens. Actuators B Chem.* **196**, 413–420 (2014)
26. Z. Wang, Z. Li, L. Liu, X. Xu, H. Zhang, W. Wang, W. Zheng, C. Wang, A novel alcohol detector based on ZrO₂-doped SnO₂ electrospun nanofibers. *J. Am. Ceram. Soc.* **93**, 634–637 (2010)
27. W. Zheng, Z. Li, H. Zhang, W. Wang, Y. Wang, C. Wang, Electrospinning route for α -Fe₂O₃ ceramic nanofibers and their gas sensing properties. *Mater. Res. Bull.* **44**, 1432–1436 (2009)
28. F. Tian, Y. Liu, K. Guo, Au nanoparticle modified flower-like ZnO structures with their enhanced properties for gas sensing. *Mater. Sci. Semicond. Process.* **21**, 140–145 (2014)
29. M. Wu, W. Zeng, Q. He, J. Zhang, Hydrothermal synthesis of SnO₂ nanocorals, nanofragments and nanoglass and their formaldehyde gas-sensing properties. *Mater. Sci. Semicond. Process.* **16**, 1495–1501 (2013)